

Article

Vibration Isolation and Alignment of Multiple Platforms on a Non-Rigid Supporting Structure

Jorge Pérez-Aracil ^{1,*}, Emiliano Pereira ^{2,*}, Sumeet S. Aphale ^{3,†} and Paul Reynolds ^{1,†}

¹ Vibration Engineering Section, College of Engineering, Mathematics and Physical Sciences, University of Exeter, Exeter EX4 4QJ, UK; p.reynolds@exeter.ac.uk

² Department of Signal Processing and Communications, Universidad de Alcalá, 28805 Alcalá de Henares, Spain

³ Center for Applied Dynamics Research, School of Engineering, University of Aberdeen, Aberdeen AB24 3UE, UK; s.aphale@abdn.ac.uk

* Correspondence: jp696@exeter.ac.uk (J.P.-A.); emiliano.pereira@uah.es (E.P.); Tel.: +44-0139-272-5821 (J.P.-A.); +44-918-85-6505 (E.P.)

† These authors contributed equally to this work.

Received: 25 August 2020; Accepted: 20 October 2020; Published: 22 October 2020



Abstract: In many applications comprised of multiple platforms with stringent vibration isolation requirements, several vibration isolators are employed to work in tandem. They usually must accomplish two objectives: (i) reduce the vibration level of each platform; and (ii) maintain the required alignment with respect to each other or with a fixed reference. If the isolators are located on a rigid supporting structure, the problem can be approached as a classical vibration isolation (VI) problem, in which an increase in damping implies a reduction of vibration level experienced by the platforms. However, there are an increasing number of scenarios in which the dynamic interaction between the isolator and the base structure has the potential to alter the system response and consequently degrade VI performance. In this work, a generalized method to analyze the combined VI and alignment problem, for multiple isolators located on a flexible supporting structure, is proposed. The dynamic interaction between the platforms and the isolators is considered in the control design, and it is proved employing two different functional values that the maximum damping solution is not always the best approach when the dynamics of the supporting structure are considered. Numerical simulations are presented to validate the theory developed and robustness of the proposed control approach is demonstrated.

Keywords: vibration control; active vibration isolation; dynamic interaction; multi-platform alignment

1. Introduction

Vibration isolation (VI) techniques are generally employed to reduce the vibrations transmitted between a supporting structure (also denoted as base) and a platform, where vibration-sensitive equipment is placed. The vibration propagation occurs via two main scenarios: Scenario 1, the equipment generates vibrations that are transferred to a supporting structure; and Scenario 2, a supporting structure propagates vibrations onto sensitive equipment it supports [1]. Vibration isolation is achieved by applying an appropriate control force that opposes the vibrations-generated force, by employing isolators that are placed between the supporting structure and the platform(s) to be isolated.

Depending on the method in which this control force is generated, three different techniques can be distinguished: Passive VI (PVI), Semi-Active VI (SAVI) and Active VI (AVI). In both PVI and SAVI, the controlled force is generated passively as a consequence of the relative movement between the supporting structure and the platform [2,3]. For PVI, the dynamic properties of the isolator system do

not change and, hence, are not able to adapt to changes in the platform and/or supporting structure dynamics. The use of SAVI can mitigate this problem, since the stiffness and/or damping of the isolator system can be varied to adapt to changes in the structural dynamics [4–6].

For both PVI and SAVI, VI only occurs for frequencies greater than $\sqrt{2}$ times the natural frequency of the isolator (i.e., its cut-off frequency). In addition, a PVI with -40 dB/dec roll-off in the isolation (or rejected) band needs a low damping ratio, which may introduce significant unwanted amplification around its resonant frequency. Nonlinear techniques have been applied to reduce the natural frequency of the isolator system, thereby improving its performance [7–14]. The problem of having less than -40 dB/dec roll-off for high frequencies when the damping ratio is reduced can be alleviated by using a spring in parallel with a Maxwell element, i.e., damper and spring in series [15]. In this approach, the damper tends to be blocked, resulting in a system with two springs in parallel.

AVI presents the following advantages: high damping ratio with -40 dB/dec roll-off in the isolation band, the possibility to reach zero static deflection, robustness to system parameter and operational uncertainties and trajectory tracking capabilities [16]. These improvements may be required in applications with highly-demanding VI requirements, such as space applications, precision research, manufacturing centres, etc. [17–20]. Thus, although the implementation cost of an AVI scheme is higher than PVI or SAVI [21–23], their advantages make AVI schemes more attractive in these applications, when compared to PVI or SAVI schemes.

In AVI, in addition to the force generated by the relative movement between the base and the platform, an additional control force is introduced, usually called *active force*. This active force is controlled by the adopting suitable feedback or feedforward control techniques [24–26]. The application of AVI implies the use of at least one sensor at the platform (feedback) or at the supporting structure (feedforward), as well as a controller and actuator to generate the control force. It is also necessary to deal with the potential problems of real-time signal processing, in particular instability problems when the system is not well modeled and/or is time variant.

If the aforementioned Scenario 2 is considered, the common hypothesis in the classic isolator system design is to consider the supporting structure as an infinitely rigid system compared with the isolator. This assumption is correct when the control force exerted by the isolation system does not significantly affect the base response [27–29]. However, this hypothesis is not valid when the movement of the supporting structure is affected by the control force, as occurs in a range of practical cases [30–37]. This interaction phenomenon, which can be defined as a hybrid scenario, may change the response of the supporting structure to perturbations, such as force exerted by other activities or displacements. Thus, vibration reduction, which may be achieved by the isolators, can also improve the isolation performance since the absolute VI level may be reduced.

An isolation system including multiple devices using a multi-input multi-output (MIMO) AVI strategy can deal with more complex problems. These MIMO AVI strategies are needed in tasks where multiple isolators are involved, such as multi-degree of freedom systems (e.g., Stewart platforms) or applications where the alignment between equipment is required [18,19,38]. Note that, if the hypothesis of a rigid base is considered, the alignment problem may be considered analogous to obtaining the best isolation performance in terms of platform movement with respect to the supporting structure. Thus, each isolator can be considered as an individual system that does not interact with other isolators or with the supporting structure. However, if the isolators are situated on a flexible supporting structure, the problem must be analyzed from a wider perspective, considering the effect that the isolator makes in the supporting structure response. This effect may involve improvements in the VI performance, as mentioned above, and in the alignment between these multiple devices. Therefore, the model used to design MIMO AVI must consider the supporting structure model, which is excited by both external disturbances and every isolator system, in order improve the performance of the isolation and alignment control objectives.

This paper studies how the control forces exerted by the isolation system may improve performance according to the isolation and alignment control objectives. Thus, under the hypothesis

of perturbation forces exerted at the supporting structure, two designs are compared. The first one considers a rigid supporting structure with no dynamic interaction with the isolator system. In this case, the best transmissibility between the accelerations of supporting structure and sensitive equipment is always the best overall solution. The second hypothesis considers a flexible supporting structure with dynamic interaction with the isolator systems. The objective of this paper is to highlight when the best AVI design does not correspond with the best transmissibility, showing the importance of considering this interaction.

The remainder of the paper continues with the general AVI framework, where a model of the isolator system placed on a flexible supporting structure is presented in order to formulate the isolation and alignment problem. Then, this general framework is particularized for a multiple single-input and single-output (SISO) AVI, which feeds back the acceleration measured at the platform of each isolator system. This section also includes the AVI control law employed and the functional used to design optimally the aforementioned real scenario. The next section includes illustrative results obtained with a large set of optimal AVI multiple SISO controllers designed for a large set of supporting structures and isolator systems. This large set of examples are normalized in terms of mass and frequency ratios of both systems. Finally, the main conclusions derived are presented.

2. General AVI Framework

This section defines a general framework where the forces generated by an isolator system together with external disturbance forces can be included into a model of the supporting structure. Thus, the performance of the isolator system, which is defined in terms of isolation and alignment, can be considered as a problem that also involves the supporting structure dynamics. Firstly, the isolator system is analyzed from a base acceleration point of view. The objective is to obtain the acceleration transmissibility between any acceleration measured at the j th isolator and the base acceleration measured at this j th location. Secondly, the base structure is modeled by considering n forces exerted by the n isolators and disturbance forces applied at l nodes of the base structure. Feedback and feedforward AVI can be included in this general model. Thirdly, this real scenario is defined in terms of isolation and alignment objectives.

2.1. Transmissibility Model for the Isolation System

Figure 1 shows the transmissibility model of the a generic isolator j , such that $\{1 \leq j \leq n, j \in \mathbb{N}\}$. The mass to be isolated is m_{p_j} , which is situated on the platform of the isolator. The dynamic properties of the isolator are modeled with its stiffness k_{p_j} and its viscous damping c_{p_j} . The active force $f_{a_j}(t)$ is obtained either by a feedback and/or feedforward technique, which may consider any variable of the isolator and/or the support. The variables $\ddot{x}_{p_j}(t)$ and $\ddot{x}_{b_j}(t)$ are the accelerations measured at m_{p_j} and at the base, respectively. If the variable $x_{r_j}(t) = x_{p_j}(t) - x_{b_j}(t)$ is defined, the differential equation describes the motion of m_{p_j} is expressed as:

$$f_{a_j}(t) - m_{p_j}\ddot{x}_{b_j}(t) = m_{p_j}\ddot{x}_{r_j}(t) + c_{p_j}\dot{x}_{r_j}(t) + k_{p_j}x_{r_j}(t) \quad (1)$$

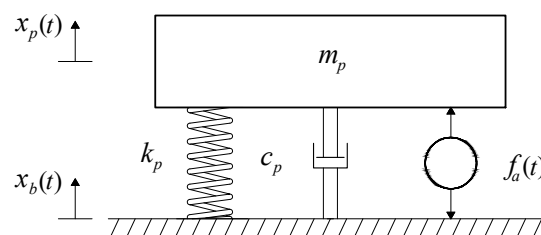


Figure 1. Single isolator on a rigid supporting system.

It is desired to have a general representation of all modeled isolator systems to formulate the design criteria. Thus, Equation (1) can be formulated as the following state–space model:

$$\begin{aligned} \dot{\mathbf{x}}_{I_j}(t) &= \mathbf{A}_{I_j}\mathbf{x}_{I_j}(t) + \mathbf{B}_{IB_j}\ddot{x}_{b_j}(t) + \mathbf{B}_{IF_j}f_{a_j}(t) \\ y_{I_j}(t) &= \ddot{x}_{p_j}(t) = \mathbf{C}_{I_j}\mathbf{x}_{I_j}(t) + \mathbf{D}_{IF_j}f_{a_j}(t), \end{aligned} \tag{2}$$

where the vector $\dot{\mathbf{x}}_{I_j}(t) = [\dot{x}_{r_j}(t), \ddot{x}_{r_j}(t)]^T$ and the matrices are hence defined as:

$$\begin{aligned} \mathbf{A}_{I_j} &= \begin{bmatrix} 0 & 1 \\ -\omega_{p_j}^2 & -2\zeta_{p_j}\omega_{p_j} \end{bmatrix}, \mathbf{B}_{IB_j} = \begin{bmatrix} 0 \\ 1 \end{bmatrix}, \mathbf{B}_{IF_j} = \begin{bmatrix} 0 \\ 1/m_{p_j} \end{bmatrix}, \\ \mathbf{C}_{I_j} &= \begin{bmatrix} -\omega_{p_j}^2 & -2\zeta_{p_j}\omega_{p_j} \end{bmatrix}, \mathbf{D}_{IF_j} = 1/m_{p_j}, \end{aligned} \tag{3}$$

in which ω_{p_j} is the natural frequency of the j th isolator, obtained by $\omega_{p_j}^2 = k_{p_j}/m_{p_j}$, and ζ_{p_j} is its damping ratio, obtained by $\zeta_{p_j} = c_{p_j}/(2m_{p_j}\omega_{p_j})$. Each isolator system then has two inputs, the base acceleration $\ddot{x}_{b_j}(t)$ and the active force $f_{a_j}(t)$, which depends on the AVI controller utilized.

If Equations (2) and (3) are generalized for the n isolators, the state–space model of the isolators system is:

$$\begin{aligned} \dot{\mathbf{X}}_I(t) &= \mathbf{A}_I\mathbf{X}_I(t) + \mathbf{B}_{IB}\ddot{\mathbf{X}}_b(t) + \mathbf{B}_{IF}\mathbf{F}_A(t), \\ \mathbf{Y}_I(t) &= \mathbf{C}_I\mathbf{X}_I(t) + \mathbf{D}_{IF}\mathbf{F}_A(t), \end{aligned} \tag{4}$$

in which the state variables of each isolator are defined in the vector $\mathbf{X}_I(t) = [x_{I_1}(t), x_{I_2}(t), \dots, x_{I_n}(t)]^T$; the output vector is $\mathbf{Y}_I(t) = [y_{I_1}(t), y_{I_2}(t), \dots, y_{I_n}(t)]^T$; the system matrix is a diagonal matrix of the system matrices of the n isolators, such that $\mathbf{A}_I = \text{diag}(\mathbf{A}_{I_1}, \mathbf{A}_{I_2}, \dots, \mathbf{A}_{I_n})$; the disturbance input matrix is $\mathbf{B}_{IB} = \text{diag}(\mathbf{B}_{IB_1}, \mathbf{B}_{IB_2}, \dots, \mathbf{B}_{IB_n})$; the controlled input matrix is $\mathbf{B}_{IF} = \text{diag}(\mathbf{B}_{IF_1}, \mathbf{B}_{IF_2}, \dots, \mathbf{B}_{IF_n})$; the output matrix is $\mathbf{C}_I = \text{diag}(\mathbf{C}_{I_1}, \mathbf{C}_{I_2}, \dots, \mathbf{C}_{I_n})$; and the feedthrough matrix is defined as $\mathbf{D}_{IF} = \text{diag}(\mathbf{D}_{IF_1}, \mathbf{D}_{IF_2}, \dots, \mathbf{D}_{IF_n})$. The inputs of the system are defined by the vectors $\ddot{\mathbf{X}}_b(t) = [\ddot{x}_{b_1}(t), \ddot{x}_{b_2}(t), \dots, \ddot{x}_{b_n}(t)]^T$ and $\mathbf{F}_A(t) = [f_{a_1}(t), f_{a_2}(t), \dots, f_{a_n}(t)]^T$.

The model of Equation (4) can be expressed in the Laplace domain as follows:

$$\mathbf{Y}_I(s) = \mathbf{G}_{IB}(s)s^2\mathbf{X}_b(s) + \mathbf{G}_{IF}(s)\mathbf{F}_A(s), \tag{5}$$

in which the variables $\mathbf{Y}_I(s)$, $\mathbf{X}_b(s)$ and $\mathbf{F}_A(s)$ are the Laplace transforms by components of the vectors $\mathbf{Y}_I(t)$, $\mathbf{X}_b(t)$ and $\mathbf{F}_A(t)$, respectively, and the matrices $\mathbf{G}_{IB}(s)$ and $\mathbf{G}_{IF}(s)$ are formed by the following transfer functions:

$$\mathbf{G}_{IB}(s) = \mathbf{C}_I [s\mathbf{I}_{2n} - \mathbf{A}_I]^{-1} \mathbf{B}_{IB}, \tag{6}$$

$$\mathbf{G}_{IF}(s) = \mathbf{C}_I [s\mathbf{I}_{2n} - \mathbf{A}_I]^{-1} (\mathbf{B}_{IF} + \mathbf{D}_{IF}), \tag{7}$$

where \mathbf{I}_{2n} is a $2n \times 2n$ identity matrix.

2.2. Supporting Structure Model

Figure 2 shows the model of the supporting structure and isolator system described in Equation (4). The supporting structure is modeled by considering n control forces, \mathbf{F}_I , exerted by the n isolators and l disturbance forces, \mathbf{F}_D , which can be applied at the isolation locations and/or at other base locations, where $l \geq 1$. The outputs of the supporting structure are the accelerations measured at the n locations of the isolators. The forces exerted by the n isolators are obtained by multiplying the vector \mathbf{Y}_I by the diagonal matrix $\mathbf{M}_P = \text{diag}(m_{p_1}, m_{p_2}, \dots, m_{p_n})$.

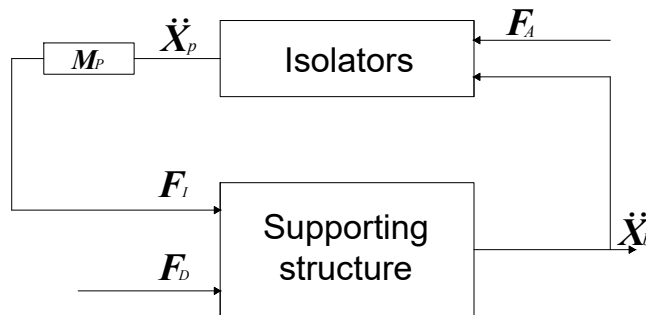


Figure 2. Schematic block diagram of the coupled isolator–structure system.

The state–space equations of the base structure of m vibration modes can be expressed as follows:

$$\begin{aligned} \dot{X}_B(t) &= A_B X_B(t) + B_{BD} F_D(t) + B_{BI} F_I(t), \\ Y_B(t) &= C_B X_B(t) + D_{BD} F_D(t) + D_{BI} F_I(t), \end{aligned} \tag{8}$$

where the matrices $A_B, B_{BD}, B_{BI}, C_B, D_{BD}$ and D_{BI} are defined as:

$$\begin{aligned} A_B &= \begin{bmatrix} \mathbf{0}_m & \mathbf{I}_m \\ -\Omega^2 & -2Z\Omega \end{bmatrix}; & B_{BD} &= \begin{bmatrix} \mathbf{0}_{m,l} \\ \Phi_D \end{bmatrix}; & B_{BI} &= \begin{bmatrix} \mathbf{0}_{m,n} \\ \Phi_I \end{bmatrix}; \\ C_B &= \Phi_I^T \begin{bmatrix} -\Omega^2 & -2Z\Omega \end{bmatrix}; & D_{BD} &= \begin{bmatrix} \Phi_I^T \Phi_D \end{bmatrix}; & D_{BI} &= \begin{bmatrix} \Phi_I^T \Phi_I \end{bmatrix}; \end{aligned}$$

The vectors $X_B(t) = [x_{B_1}(t), \dot{x}_{B_1}(t), \dots, x_{B_m}(t), \dot{x}_{B_m}(t)]^T$, $F_D(t) = [f_{d_1}(t), \dots, f_{d_l}(t)]^T$ and $F_I(t) = [f_{I_1}(t), \dots, f_{I_n}(t)]^T = M_P Y_I(t)$ are the state–space vector, the disturbance force and the forces exerted by the n isolators, respectively. The output vector is $Y_B(t) = \ddot{X}_b(t) = [\ddot{x}_{b_1}(t), \dots, \ddot{x}_{b_n}(t)]^T$. Note that $\ddot{x}_{b_j}(t)$ is the acceleration measured in the j th isolator location and $x_{B_q}(t)$ is the modal state variable of the q th mode, which is used to define the state vector $X_B(t)$ of the supporting structure.

The terms $\Omega = \text{diag}(\omega_{b_1}, \dots, \omega_{b_m})$ and $Z = \text{diag}(\zeta_{b_1}, \dots, \zeta_{b_m})$ are $m \times m$ diagonal matrices formed by the natural frequencies of the structure and the damping ratios. The matrices $\mathbf{0}_m$ and \mathbf{I}_m are the zero and identity matrices of dimension $m \times m$, while $\mathbf{0}_{m,l}$ and $\mathbf{0}_{m,n}$ represent $m \times l$ and $m \times n$ zero matrices, respectively. Φ_D is a $m \times l$ matrix whose columns are the mode shapes at the disturbance locations, while Φ_I is a $m \times n$ matrix whose columns are formed by the mode shapes of the supporting structure at the isolator locations.

The model of Equation (8) can be expressed in the Laplace domain as follows:

$$Y_B(s) = s^2 X_b(s) = G_{BD}(s) F_D(s) + G_{BI}(s) Y_I(s), \tag{9}$$

in which the variables $Y_B(s)$ and $F_D(s)$ are the Laplace transforms of $Y_B(t)$ and $F_D(t)$, respectively, and the matrices $G_{BD}(s)$ and $G_{BI}(s)$ are formed by the following transfer functions:

$$G_{BD}(s) = C_B [sI_{2m} - A_B]^{-1} B_{BD} + D_{BD}, \tag{10}$$

$$G_{BI}(s) = (C_B [sI_{2m} - A_B]^{-1} B_{BI} + D_{BI}) M_P, \tag{11}$$

where I_{2m} is a $2m \times 2m$ identity matrix of the same dimensions as A_B .

If Equation (9) is substituted into Equation (5), the accelerations of the isolator masses are given by:

$$\begin{aligned} Y_I(s) &= [I_n - G_{IB}(s) G_{BI}(s)]^{-1} G_{IB}(s) G_{BD}(s) F_D(s) + \\ & [I_n - G_{IB}(s) G_{BI}(s)]^{-1} G_{IF}(s) F_A(s), \end{aligned} \tag{12}$$

which depend on the disturbance forces (F_D) and the active forces (F_A). This equation is needed to study the influence of the platform acceleration when a non-rigid supporting structure, an AVI and disturbance forces are considered together. Then, the AVI objectives are defined as: (i) transmissibility defined by Equation (5) ($Y_{I_j}(s)/Y_{B_j}(s)$); and (ii) the alignment between two platforms in the presence of the disturbance force, which can also be defined from Equation (12) ($(Y_{I_j}(s) - Y_{I_{j+1}}(s))/F_{d_k}(s)$). The variables $Y_{I_j}(s)$, $Y_{B_j}(s)$ and $F_{d_k}(s)$ are components of the vectors $Y_I(s)$, $Y_B(s)$ and $F_D(s)$, respectively.

2.3. Formulation of the VI and Alignment Problem

The objectives of the AVI defined in this section consider the maximum value of the frequency response functions defined by $Y_{I_j}(s)/Y_{B_j}(s)$ and $(Y_{I_j}(s) - Y_{I_{j+1}}(s))/F_{d_k}(s)$. Thus, the following variables are defined: (i) the transmissibility between the platform and supporting structure acceleration, defined in this work as:

$$\Lambda_T = \frac{1}{n} \sum_{j=1}^n \left\| \frac{Y_{I_j}(s)}{Y_{B_j}(s)} \right\|_{\infty} ; \tag{13}$$

and (ii) the alignment of the isolators located on the supporting structure, which is illustrated in Figure 3, and defined as follows:

$$\Lambda_A = \frac{1}{l(n-1)} \sum_{j=1}^{n-1} \frac{\sum_{k=1}^l \left\| \frac{Y_{I_j}(s) - Y_{I_{j+1}}(s)}{F_{d_k}(s)} \right\|_{\infty}}{L_{j,j+1}}. \tag{14}$$

The expression of Equation (14) is based on the tangent of the angle between adjacent platforms, $\tan \theta_{j,j+1}$. The angle has been considered to be small enough such that $\tan(\theta_{j,j+1}) \approx \theta_{j,j+1}$.

As can be observed, both expressions are divided by the number of addends, thus the functional values can be compared independently of the number of isolators and disturbance forces applied on the supporting structure.

The design criterion based on a rigid supporting structure hypothesis considers AVI that minimizes Λ_T defined by Equation (13). The design criterion based on a flexible supporting structure considers the AVI objectives defined by the combination of Λ_T and Λ_A .

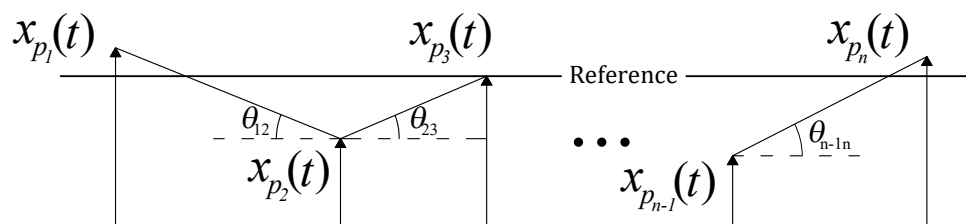


Figure 3. Illustration of the alignment problem.

3. Interaction Problem Using a Feedback AVI Control Law

This section particularizes Equations (5) and (12) when the AVI is based on the following feedback strategy:

$$F_A(s) = G_{AVI,F}(s)Y_I(s), \tag{15}$$

where $G_{AVI,F}(s)$ is the matrix formed by the transfer functions that relate the n outputs of the isolator system with the n inputs. Thus, if Equation (15) is considered, Equations (5) and (12) are as follows:

$$Y_I(s) = [I_n - G_{IF}(s)G_{AVI,F}(s)]^{-1} G_{IB}(s)Y_B(s), \tag{16}$$

$$Y_I(s) = \left[I_n - [I_n - G_{IB}(s)G_{BI}(s)]^{-1} G_{IF}(s)G_{AVI,F}(s) \right]^{-1} \cdot [I_n - G_{IB}(s)G_{BI}(s)]^{-1} G_{IB}(s)G_{BD}(s)F_D(s). \tag{17}$$

Then, Equation (16) is used to obtain the variable defined in Equation (13), and Equations (16) and (17) are used to obtain the variables defined in Equation (14).

AVI Control Law

The matrix $G_{AVI,F}(s)$ is defined as follows:

$$G_{AVI,F}(s) = \begin{bmatrix} C_{f_1}(s) & \dots & 0 \\ \vdots & \ddots & \vdots \\ 0 & \dots & C_{f_n}(s) \end{bmatrix} = \frac{1}{s} \begin{bmatrix} k_{v_1} & \dots & 0 \\ \vdots & \ddots & \vdots \\ 0 & \dots & k_{v_n} \end{bmatrix} = \frac{1}{s} K_V, \tag{18}$$

where c_{f_j} is considered in this work as a direct velocity feedback (DVF), with the aim to emulate the behavior of a *sky-hook* damper [1], in which each force $f_{a_j}(t)$ only depends on the movement of the platform. The active damping added to the isolator by the DVF $c_{f_j}(s)$ increases with the absolute value of the gain k_{v_j} . The DVF controller of the j th isolator can be expressed as:

$$C_{f_j}(s) = k_{v_j}/s, \tag{19}$$

in which k_{v_j} is the controller gain. The matrix of the isolator system of Equation (18) is given by $K_V = \text{diag}(k_{v_1}, \dots, k_{v_n})$. The transfer function between the platform acceleration (\ddot{x}_{p_j}) and the base acceleration (\ddot{x}_{b_j}) for the j th isolator (Figure 1) and the DVF of Equation (19) is as follows:

$$\frac{s^2 X_{p_j}(s)}{s^2 X_{b_j}(s)} = \frac{2\zeta_{p_j}\omega_{p_j}s + \omega_{p_j}^2}{s^2 + 2\zeta_{p_j}\omega_{p_j}s + \omega_{p_j}^2 - (k_{v_j}/m_{p_j})s}. \tag{20}$$

Note that the value of ζ_{p_j} should be small enough to guarantee a -40 dB/dec attenuation in first part of the rejected band. For example, if the value of ζ_{p_j} is equal to 0.01, there is a -40 dB/dec attenuation between ω_{p_j} and $50\omega_{p_j}$ (i.e., the zero is placed at $-50\omega_{p_j}$). The objective of Equation (20) is to increase the damping of the poles, reducing the peak response. The value of this closed-loop damping, denoted in this work as $\zeta_{p_j}^{AVI}$, is obtained with following equation:

$$\zeta_{p_j}^{AVI} = \zeta_{p_j} - \frac{k_{v_j}}{2m_{p_j}\omega_{p_j}}. \tag{21}$$

4. Application Example

In this section, the analysis of the VI and the alignment problem is particularized to the case of three isolators placed on a simply supported beam. The numerical results illustrate when the dynamics of the supporting structure must be considered in the alignment problem (i.e., the combination of Λ_T and Λ_A). This section is divided into: (i) system dynamics; (ii) design criterion; (iii) numerical examples for symmetrical and non-symmetrical configurations of the three isolators; and (iv) robustness analysis for isolator parameter uncertainty.

The system configuration adopted here represents a general case study, in which the isolators are situated on the same non-rigid supporting structure. Similar configurations can be found in [31,39], in which four actuators are used to isolate the equipment situated on a flexible supporting plate structure. An identical configuration considering only one isolator is also presented in [40].

4.1. System Dynamics

The system can be divided into two parts: the supporting structure and the three isolators (Figure 4). The first is chosen to be a pinned-pinned supported beam. The relevant beam material properties are Young’s modulus (E_x) and its density (ρ). The geometrical properties of the beam are defined such that the inertia of the cross-section with respect to the horizontal axis is I_x and the length between the supports is L_b .

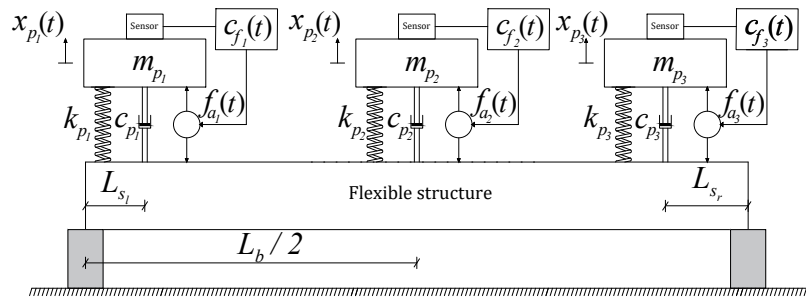


Figure 4. Illustration of three isolators situated on a flexible beam support.

The q th mode shape of the beam can be expressed as [41]:

$$\phi_{b_q}(x) = C_1 \sin \frac{q\pi x}{L_b}, \tag{22}$$

in which C_1 is a constant that has been chosen to be unity. The frequency of the q th mode can be expressed as:

$$\omega_{b_q} = \left(\frac{q\pi}{L_b} \right)^2 \sqrt{\frac{E_x I_x}{M_L}}, \tag{23}$$

in which M_L is the mass per unit length of the beam. The relationship between the vibration modal frequencies can be defined by considering Equation (23) as: $\omega_{b_q} = \omega_{b_1} \cdot q^2$, in which $1 \leq q \leq m$.

The variables L_{s_1} and L_{s_r} are the distances from the end isolators with respect to the left and right supports, respectively, and they correspond with the location of the isolators $j = 1$ and $j = 3$, respectively. The isolator $j = 2$ has been considered to be at the mid-span of the beam structure for the symmetrical and non-symmetrical cases. The distances used for the functional are $L_{12} = L_b/2 - L_{s_1}$ and $L_{23} = L_b/2 - L_{s_r}$.

The state–space representation proposed in Equation (8) is used to model the supporting structure, in which: (i) the number of modes considered for the analysis is $m = 3$; (ii) the number of inputs of the isolator system (i.e., the number of outputs of the supporting structure) is $n = 3$; (iii) the considered disturbance forces are at the isolation locations ($l = 3$) or one force located at $L_b/4$ from the left support, which can excite all the considered vibration modes ($l = 1$); and (iv) the damping is assumed to be constant for all modes, with a value of $\zeta_{b_q} = 0.005$, in which $1 \leq q \leq 3$.

The three isolators are considered to have the same dynamic properties (i.e., the values of m_{p_j} , ω_{p_j} and ζ_{p_j} are the same for $j = 1, 2, 3$). The values of the masses and natural frequencies are defined with respect to the supporting structure model as follows:

$$m_{p_j} = r_m M_m, \tag{24}$$

$$\omega_{p_j} = r_\omega \omega_{b_1}, \tag{25}$$

where r_m is the ratio between the isolator mass and the beam modal mass, which is defined as $M_m = M_L L_b/2$, and r_ω is the ratio between natural frequency of the isolator and the first vibration mode of the beam. The simulations have been developed considering $\zeta_{p_1} = \zeta_{p_2} = \zeta_{p_3} = 0.01$.

4.2. Design Criterion

The design criterion is based on finding the optimal gains values k_{v_1} , k_{v_2} and k_{v_3} for each pair of values r_m and r_ω to minimize the following functional:

$$f_{fv}(\mathbf{K}_V, r_m, r_\omega) = \alpha \Lambda_T(\mathbf{K}_V, r_m, r_\omega) + \beta M_m L_b \Lambda_A(\mathbf{K}_V, r_m, r_\omega), \tag{26}$$

where the parameters α and β balance the importance of vibration level reduction for every platform, which is defined by Λ_T , and the relative alignment between the isolators, which is defined by Λ_A . In this particular example, these parameters are considered as $\alpha = \beta = 0.5$. Note that: (i) the function Λ_T depends on \mathbf{K}_V , r_m , and r_ω ; and (ii) the function Λ_A is scaled by $M_m L_b$ to make f_{fv} independent of the flexible beam, depending only on \mathbf{K}_V , r_m and r_ω . Thus, the conclusions can be generalized to any simply supported beam where such configurations of isolator systems are used, simplifying a future experimental validation.

Firstly, if the rigid case is considered, the minimization of the functional value f_{fv} is simplified to the minimization of Λ_T . Thus, the optimal value of \mathbf{K}_V must be as large as possible. To limit this value, this work considers that the maximum damping in this numerical example is one. Thus, the gain k_{v_j} obtained for this damping value, which is denoted as \hat{k}_{v_j} , is calculated as follows:

$$\hat{k}_{v_j} = -2(1 - \zeta_{p_j}) m_{p_j} \omega_{p_j}, \tag{27}$$

where the optimal matrix for the rigid case is defined as $\hat{\mathbf{K}}_V$. Secondly, the flexible supporting structure is also considered in order to minimize Equation (26). The optimal value of \mathbf{K}_V is denoted as $\hat{\mathbf{K}}_{FV}$. Thus, the differences in $f_{fv}(\hat{\mathbf{K}}_V) / f_{fv}(\hat{\mathbf{K}}_{FV})$, which must be greater or equal to one, and $\mathbf{K}_V / \mathbf{K}_{FV}$, where each component must be also be greater than or equal to one, are useful to illustrate and quantify the interaction between the supporting structure and isolator system in terms of isolation and alignment objectives. Note that the damping of the transmissibility for $\hat{\mathbf{K}}_{FV}$ will be always less than or equal to that obtained with $\hat{\mathbf{K}}_V$, showing that a worse transmissibility may improve the alignment objective.

4.3. Numerical Results

Since the functional $f_{fv}(\mathbf{K}_V, r_m, r_\omega)$ does not depend on M_m and L_b , the value of L_b is 1 [m], while the modal mass of the supporting structure has been chosen to be 10 kg. The range of the ratios for r_m and r_ω are defined in Table 1. The value of each k_{v_j} must be between \hat{k}_{v_j} and zero.

Table 1. Mass ratios r_m and frequency ratios r_ω used in the numerical experiment.

r_m	r_ω
$[1 \cdot 10^{-4}, 1.5]$	$[0.1, 1.5]$

Two examples are presented: (i) a symmetrical case with $L_{s_l} = L_{s_r} = L_b/4$ ($L_{12} = L_{23} = L_b/4$); and (ii) a non-symmetrical case with $L_{s_l} = L_b/4$ and $L_{s_r} = L_b/6$ ($L_{12} = L_b/4$ and $L_{23} = L_b/3$). In addition, two scenarios are independently studied in order to compare the effect of disturbance force location. The first considers a single disturbance force applied at $L_b/4$. The second considers three disturbances forces applied at the isolator locations. The optimal control gains for each case have been obtained using the Nelder–Mead simplex algorithm [42] with boundary conditions [43]. The maximum number of iterations has been chosen to be 2000, with a tolerance on convergence of 10^{-6} . Additionally, the stability of the overall system defined in Equations (9), (16) and (17) is verified. Thus, if there are positive real poles, the functional defined in Equation (26) is penalized and all unstable solutions are discarded.

With the aim of showcasing the effect of uncertainty in isolator dynamics on the VI and alignment performance, a robustness analysis has been conducted. The single force disturbance input case is

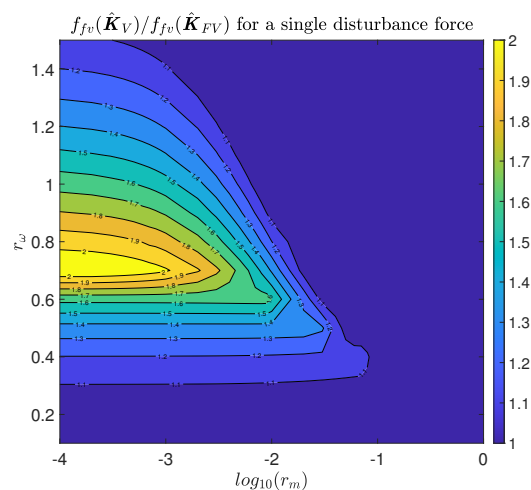
analyzed for symmetrical and non-symmetrical scenarios, considering variations of 5% and 10% in the dynamic properties ζ_{p2}, ω_{p2} , of the mid-span isolator.

4.3.1. Symmetrical Case: $L_{12} = L_{23} = L_b/4$

A comparison of the functional $f_{fv}(\mathbf{K}_V)$ for both optimal control gains $\hat{\mathbf{K}}_V, \hat{\mathbf{K}}_{FV}$ is shown in Figure 5. Figure 5a shows the case of a single disturbance force, which is applied at $L_b/4$ from the left support, and Figure 5b shows the three disturbance forces applied at the isolator locations.

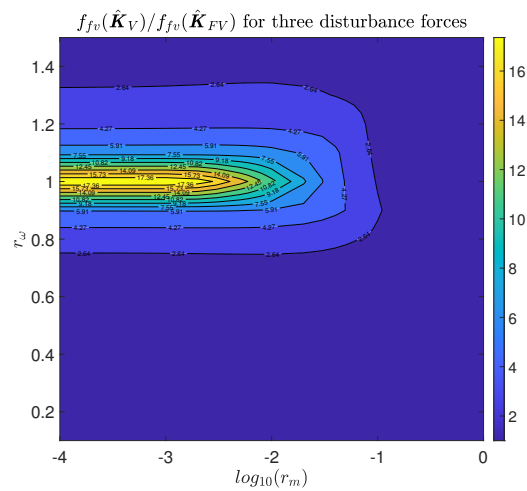
The influence of the frequency ratio r_ω is much higher than the influence of the mass ratio r_m for the scenario of a single disturbance force. The highest influence region is determined for $r_\omega \rightarrow 0.8$ and low mass ratios. The use of $\hat{\mathbf{K}}_V$ may imply an increment of two times the value of $f_{fv}(\mathbf{K}_V)$ with respect to the use of $\hat{\mathbf{K}}_{FV}$. It is important to note that, for most of the domain analyzed here, the influence of the dynamics of the supporting structure on the functional value is high. This influence starts to be significant from $r_m \leq 0.1$. In addition, the interval for r_ω is between 0.3 and 1.5, when $r_m = 10^{-4}$, where the functional varies from 9% to 200%.

Before analyzing the case of three disturbance forces applied at the isolator locations, it should be noted that the total effect of the force applied at isolators 1 and 3 is null and the force applied at isolator 2 does not excite the second mode. Thus, the second mode of the flexible support does not affect Equation (26). Therefore, the three gains of the isolators must be tuned to find a trade-off between the transmissibility and the cancellation of the first and third mode. Thus, the improvement must be more important than for a single disturbance force, which excites the three vibration modes. This is evidenced in Figure 5b, where the ratio $f_{fv}(\hat{\mathbf{K}}_V)/f_{fv}(\hat{\mathbf{K}}_{FV})$ is shown. For most of the region, the use of $\hat{\mathbf{K}}_V$ implies an increment of the functional value two times higher than the use of $\hat{\mathbf{K}}_{FV}$. In addition, if the frequency of the isolators are similar to the first natural frequency of the supporting structure, the influence of the base dynamic on the functional value is higher, reaching an increment of nineteen times higher if $\hat{\mathbf{K}}_V$ is used. Note that this increment shows that the isolators are working as tuned mass dampers tuned to the resonant frequency of the first vibration mode of the base supporting structure. Note that the difference between an isolator system optimally tuned to damp the first vibration mode respect to other tuned to minimize Δ_T , with $\zeta_{p_j}^{AVI} = 1$, is more significant for low values of r_m . This justifies that the maximum difference occurs for $r_m = 10^{-4}$.



(a)

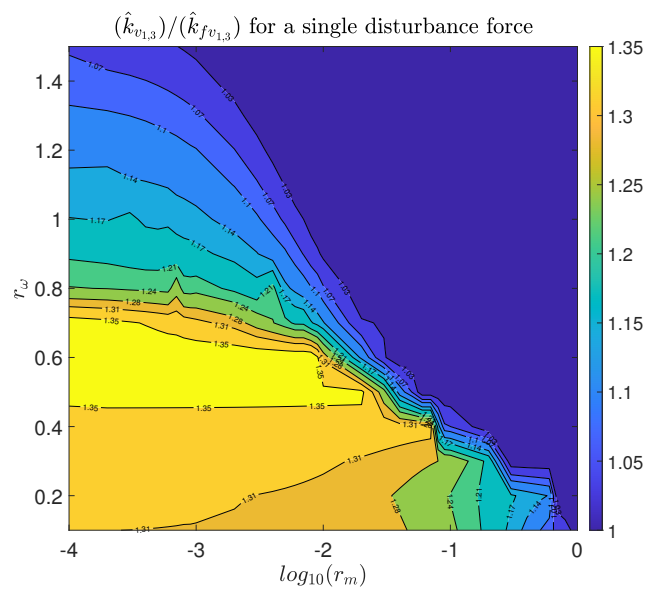
Figure 5. Cont.



(b)

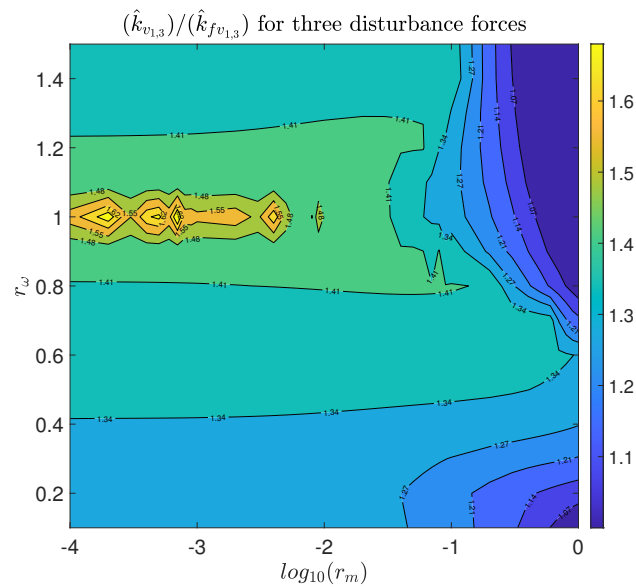
Figure 5. Ratio $f_{f_v}(\hat{K}_V)/f_{f_v}(\hat{K}_{FV})$ for: (a) a single disturbance force; and (b) three disturbance forces for the symmetrical case.

The functional value $f_{f_v}(\mathbf{K}_V)$ is determined by the control gains. It must be highlighted that, for most of the domain analyzed in this work, the optimal control gain found is not the one that implies maximum damping ($\zeta_{p_j}^{AVI} = 1$). Figure 6a shows the ratio \hat{K}_V/\hat{K}_{FV} when a single disturbance force is applied, while Figure 6b shows the same ratio when three disturbance forces are applied. In both scenarios, the highest gain reduction region is almost coincident with the highest influence region of $f_{f_v}(\hat{K}_V)/f_{f_v}(\hat{K}_{FV})$. Hence, the compromise between alignment and VI is shown, since considerable reductions in Λ_A are achieved with values of $\zeta_{p_j}^{AVI}$ less than one.



(a)

Figure 6. Cont.



(b)

Figure 6. Ratio $\hat{k}_{v_{1,3}}/\hat{k}_{f_{v_{1,3}}}$ for: (a) a single disturbance force; and (b) three disturbance forces for the symmetrical case.

Next, the impulse responses of $(y_{I_1}(t) - y_{I_2}(t))$ are compared for three particular cases of r_ω and r_m to illustrate the importance of considering the supporting structure dynamics in the control design problem.

For the cases $r_m = 0.01$, $r_\omega = 0.3$, the ratios $f_{fv}(\hat{K}_V)/f_{fv}(\hat{K}_{FV})$ are 1.08 and 1.09 for a single and three disturbance inputs, respectively. A small improvement in the temporal responses can be seen in Figure 7a,d.

For the cases $r_m = 0.001$, $r_\omega = 0.5$, which are shown in Figure 7b,e, the ratios $f_{fv}(\hat{K}_V)/f_{fv}(\hat{K}_{FV})$ are 1.35 and 1.37 for a single and three disturbance inputs, respectively. An appreciable change in the time response can be appreciated in these temporal responses.

For the cases $r_m = 0.0001$, $r_\omega = 0.9$, which are shown in Figure 7c,f, the ratios $f_{fv}(\hat{K}_V)/f_{fv}(\hat{K}_{FV})$ are 1.80 and 6.34 for a single and three disturbance inputs, respectively. A high influence of the supporting structure dynamic into the time response can be seen. Note the considerable reduction for the scenario with three disturbance inputs.

Finally, it should be noted that there are two effects. The first one is associated with the level of vibration, which depends mainly on the synchronization of isolators 1 and 2 and their transmissibility. In this case, the response of $(y_{I_1}(t) - y_{I_2}(t))$ is reduced in amplitude but its settling time is not significantly changed (i.e., the damping imparted to the vibration modes is not significant). For example, in Figure 7b,e, the setting time is slightly increased but the amplitude is reduced. The second one is associated with the damping imparted to the supporting structure, which reduces the settling time of the response $(y_{I_1}(t) - y_{I_2}(t))$. This can be clearly seen in Figure 7c,f, as explained in Figure 5b comments. Therefore, these behaviors, which depend on the interaction between the isolator system and the supporting structure, are not obvious and must be considered when a dual VI and alignment problem is being examined.

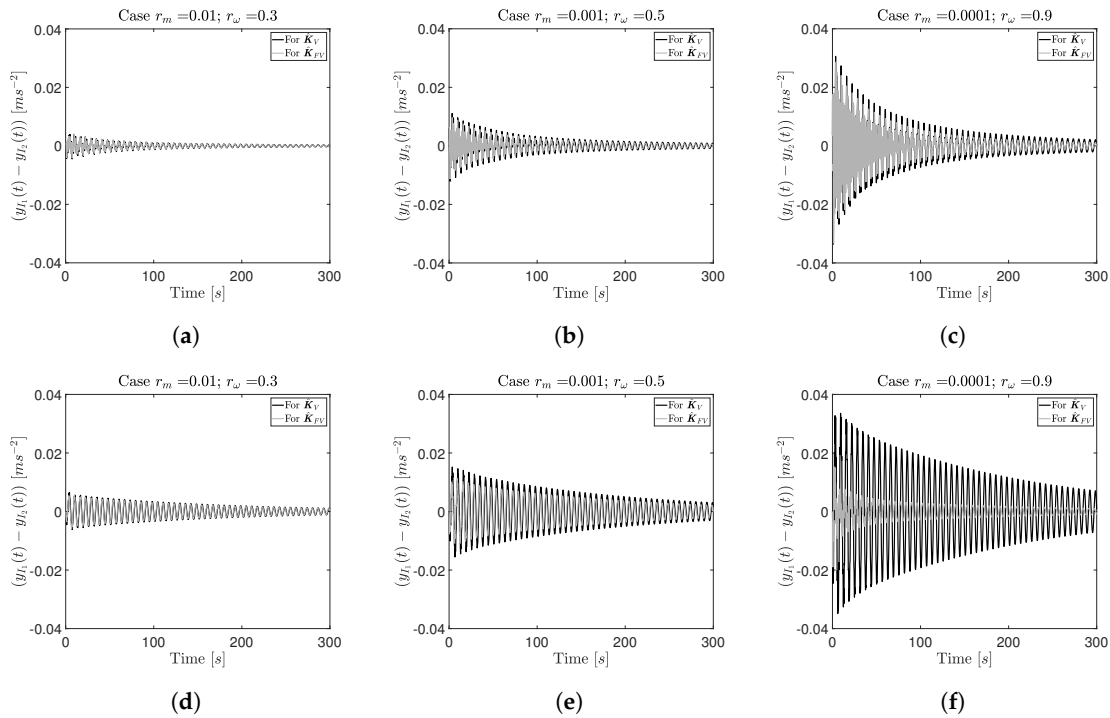


Figure 7. Impulse responses for three particular cases: ($r_m = 0.01, r_\omega = 0.3$) (a,d); ($r_m = 0.001, r_\omega = 0.5$) (b,e); and ($r_m = 0.0001, r_\omega = 0.9$) (c,f), for a single disturbance input (top row) and three disturbance inputs for the symmetrical case (bottom row).

4.3.2. Non-Symmetrical Case: $L_{12} = L_b/4$ and $L_{23} = L_b/3$

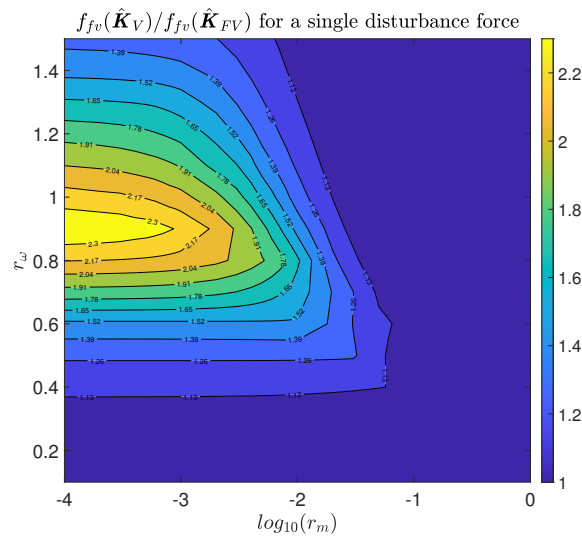
In this subsection, the case in which the end isolators are located asymmetrically with respect to the mid-span isolator is studied. The distances have been defined to be at the maximum amplitude location for the three first vibration modes, i.e., $L_{s_1} = L_b/4, L_{s_r} = L_b/6$. The objective of including this case is to show how the position of the isolators in the supporting structure can also affect the task performance. Note that the contribution of the disturbance forces and the isolators to the vibration modes of the base supporting structure are different with respect to the symmetrical case.

The influence of the supporting structure dynamics on the functional $f_{fv}(\hat{K}_V)$ is analyzed for a single disturbance force applied at $L_b/4$ (Figure 8a). In this case, the first difference observed with respect to the symmetric all case is the change in the highest influence region, which is observed for $r_\omega \rightarrow 0.9$. The influence of mass ratios seems to be slightly higher than for the symmetrical case. In addition, the maximum value of the functional ratio $f_{fv}(\hat{K}_V)/f_{fv}(\hat{K}_{FV})$ is greater than in the symmetrical case.

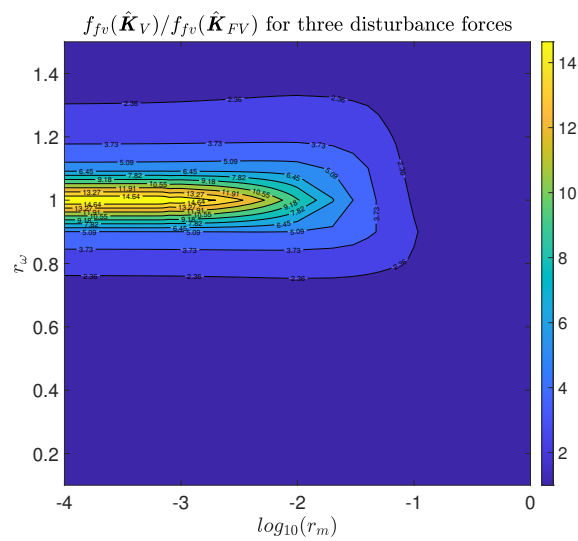
In this case, the three disturbance forces can excite the three vibration modes. However, the forces applied to L_{s_1} and L_{s_r} do not excite the second vibration mode significantly in comparison with the first and the third vibration modes. Thus, its contribution is not significant in Equation (26). In addition, the contribution to the third vibration mode is more significant in Equation (26), with respect to the symmetrical case. Thus, the improvement in the ratio $f_{fv}(\hat{K}_V)/f_{fv}(\hat{K}_{FV})$ is less important in this example, as shown in Figure 8b. Note also that the maximum influence region is similar to that of the symmetrical case. The highest ratio values of $f_{fv}(\hat{K}_V)/f_{fv}(\hat{K}_{FV})$ are lower than for the symmetrical case.

Another difference with respect to symmetrical case is that both end isolators ($j = 1$ and $j = 3$) have different optimal control gains, since their locations with respect to the mid-span isolator are different. The comparisons between \hat{k}_{fv_1} and \hat{k}_{v_1} and between \hat{k}_{fv_3} and \hat{k}_{v_3} are shown in Figure 9a for one disturbance force scenario. For the left isolator ($j = 1$), the optimal gain value \hat{k}_{fv_1} can be reduced more than 1.40 times the gain value \hat{k}_{v_1} . For the right isolator, the optimal control gain considering the supporting structure dynamic \hat{k}_{fv_3} may be reduced more than 1.90 times the gain value \hat{k}_{v_3} . In both

cases, a considerably reduction of the damping ratio is achieved. The same comparisons for the three disturbance force scenario is shown in Figure 9b. It is observed that the influence of the mass ratio is much higher than for a single disturbance force. For the left isolator, the optimal control gain \hat{k}_{fv_1} can be even 1.60 lower than \hat{k}_{v_1} . For the right isolator, the ratio $\hat{k}_{fv_3}/\hat{k}_{v_3}$ can be higher than 2.



(a)



(b)

Figure 8. Ratio $f_{fv}(\hat{K}_V)/f_{fv}(\hat{K}_{FV})$ for: (a) a single disturbance force; and (b) three disturbance forces for the non-symmetrical case.

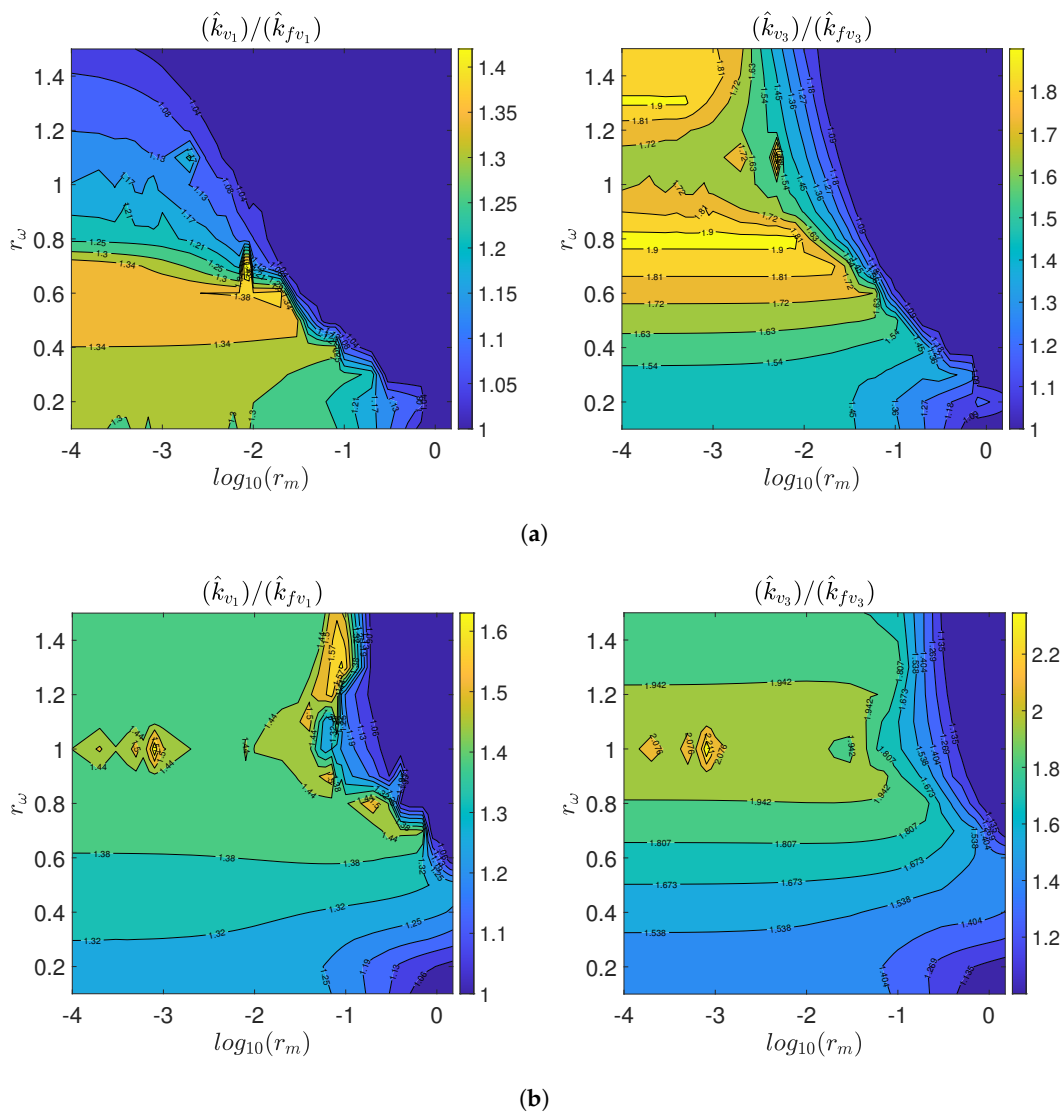


Figure 9. Ratios $\hat{k}_{v1}/\hat{k}_{fv1}$ and $\hat{k}_{v3}/\hat{k}_{fv3}$ for: (a) a single disturbance force; and (b) for three disturbance forces for the non-symmetrical case.

The same strategy of examining impulse response functions of the tangent is followed here to demonstrate the beneficial effect of using the optimal control gain \hat{K}_{FV} for the alignment problem. The same pairs (r_m, r_ω) were used in the symmetrical case are analyzed here.

For the case $r_m = 0.01$, $r_\omega = 0.3$, the relative alignment between left and mid-span isolators is observed in an impulse response in Figure 10a,d. For this case, the influence of the supporting structure is not very high, with $f_{fv}(\hat{K}_V)/f_{fv}(\hat{K}_{FV}) = 1.06$ for one disturbance input and $f_{fv}(\hat{K}_V)/f_{fv}(\hat{K}_{FV}) = 1.07$ when three disturbances inputs are applied. However, it is observed in both temporal responses that the use of \hat{K}_{FV} slightly improves the alignment.

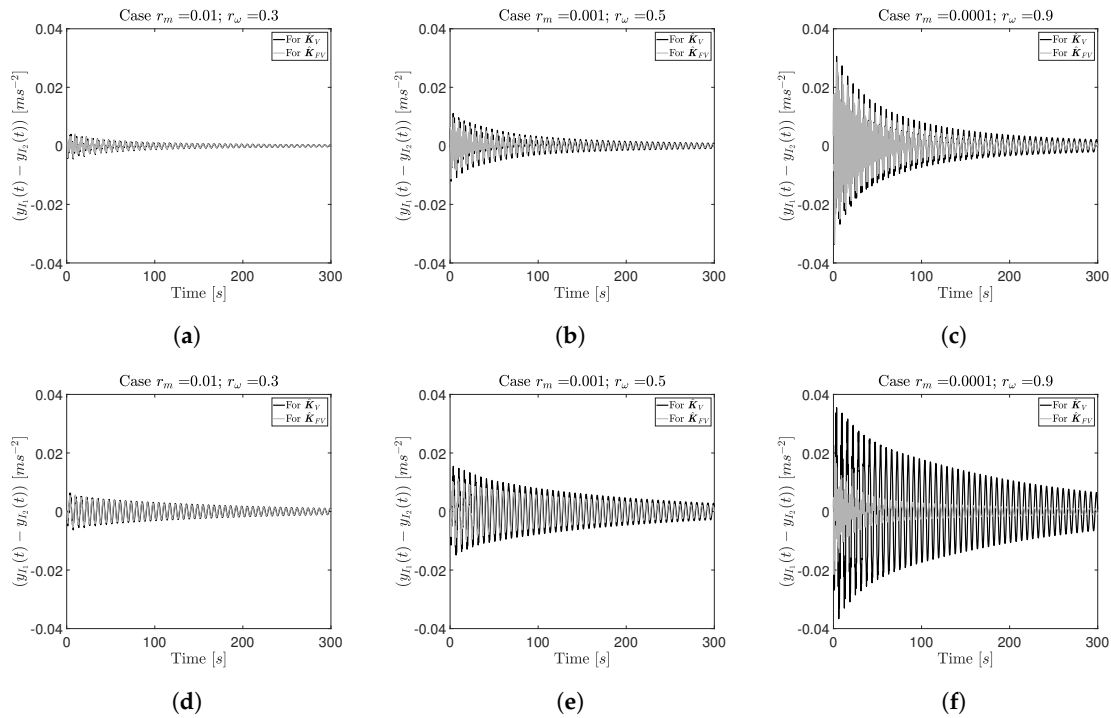


Figure 10. Impulse responses for three particular cases: ($r_m = 0.01, r_\omega = 0.3$) (a,d); ($r_m = 0.001, r_\omega = 0.5$) (b,e); and ($r_m = 0.0001, r_\omega = 0.9$) (c,f), for a single disturbance input (top row) and three disturbance inputs for the non-symmetrical case (bottom row).

For the pair $r_m = 0.001, r_\omega = 0.5$, the difference of considering \hat{K}_V or \hat{K}_{FV} is clearly highlighted in Figure 10b for a single disturbance force, in which the functional ratio $f_{fv}(\hat{K}_V)/f_{fv}(\hat{K}_{FV})$ is equal to 1.27. If three disturbance forces are considered, this ratio is equal to 1.29, and the effect in the alignment problem is shown in Figure 10e. Note that the settling time for the three disturbance forces is higher than for the single disturbance force case.

For the pair $r_m = 0.0001, r_\omega = 0.9$, the value of $f_{fv}(\hat{K}_V)/f_{fv}(\hat{K}_{FV})$ is equal to 2.38 for a single disturbance force and 5.28 for three disturbance forces. In Figure 10c,f, the alignment problem is improved for \hat{K}_{FV} . Figure 10f shows that the settling time is also reduced, and considering the supporting structure dynamics clearly improves the functional value.

4.3.3. Robustness Analysis

In practical applications, the identified models always encounter uncertainty in model parameters. Moreover, these parameters can be time variant over the operational lifetime and affect to the stability of any adopted AVI scheme. As a result, incorporating adequate robustness to system parameter uncertainty is key to the design and implementation of any AVI scheme. Consequently, to conclude this work, a robustness analysis of the proposed method has been conducted. The nominal values for system parameters—damping ratio and natural frequency of the mid-span isolator (ζ_{p_2} and ω_{p_2})—are both varied by 5% and 10% in each case, and the AVI performance, alignment and stability are quantified. The first main conclusion of this analysis is that the proposed AVI scheme is always stable across the uncertainty zone. The second conclusion is that f_{fv} can vary significantly when ζ_{p_2} and ω_{p_2} change. Additionally, the value of f_{fv} for the rigid base is either equal to or greater than that for the non-rigid base (improved performance).

The three parameter value sets for r_m and r_ω for symmetrical and non-symmetrical cases and a single disturbance force analyzed are: (i) $r_m = 0.01, r_\omega = 0.3$; (ii) $r_m = 0.001, r_\omega = 0.5$; and (iii) $r_m = 0.0001, r_\omega = 0.9$. Note that the parameter r_ω varies when ω_{p_2} changes. The value of $\zeta_{p_2}^{AVI}$ depends of ω_{p_2} and ζ_{p_2} . Therefore, the nominal case is not the optimum for this robustness analysis. In other words, the values for f_{fv} can be reduced when the parameters ζ_{p_2} and ω_{p_2} change.

Figure 11 shows the effect on the VI and alignment performance for the symmetrical case. For the first case, the robustness analysis is shown in Figure 11a,d. It is observed that, if the value of the parameters of the mid-span isolator are reduced, the response is improved and vice versa. This is because the control gain limits are not changed. However, in both cases, considering the dynamics of the supporting structure improves the VI and alignment performance.

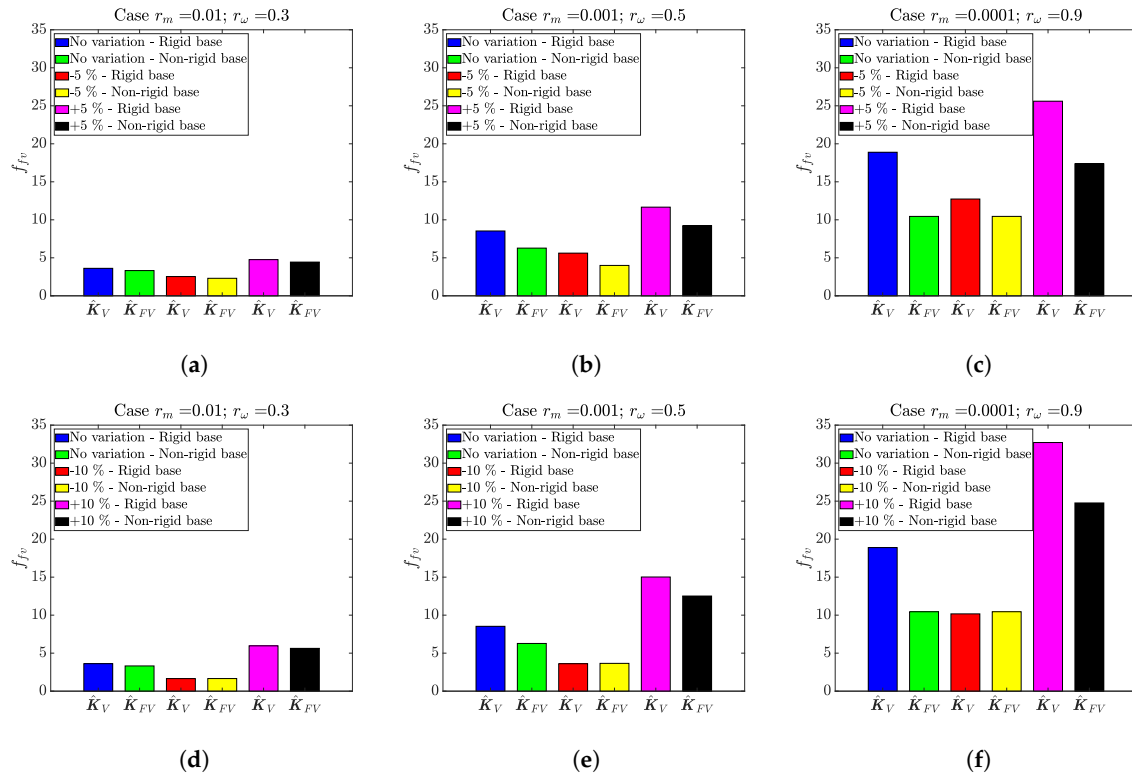


Figure 11. Effect on the VI and alignment performance due to 5% (a–c) and 10% variation (d–f) in system parameters $\zeta_{p_2}, \omega_{p_2}$ of the mid-span isolator—symmetrical case.

Similar behavior is encountered for the second case, as shown in Figure 11b,e. As expected, for a higher variation in the dynamic properties of the mid-span isolator, the performance is more different respect to the ideal case (no variation). It can be observed in the the third scenario (Figure 11c,f) that, although the functional value is high for the ideal case (no variation), considering the dynamic of the supporting structure improves the performance even though the controller is not designed considering uncertainty in the dynamic properties of the isolator.

For the non-symmetrical case, similar behavior is observed for the first case (see Figure 12a,d). As the control gain limits are maintained, performance improvement is seen when parameter values are reduced when compared to the nominal case. The performance of the VI and alignment performance is worsened compared to the ideal case when the parameters are increased. However, in both cases, considering the dynamics of the supporting structure improves the response.

For the second (Figure 12b,e) and third (Figure 12c,f) cases, similarity to the symmetrical case is found, hence showing the importance of considering the dynamic of the supporting structure.

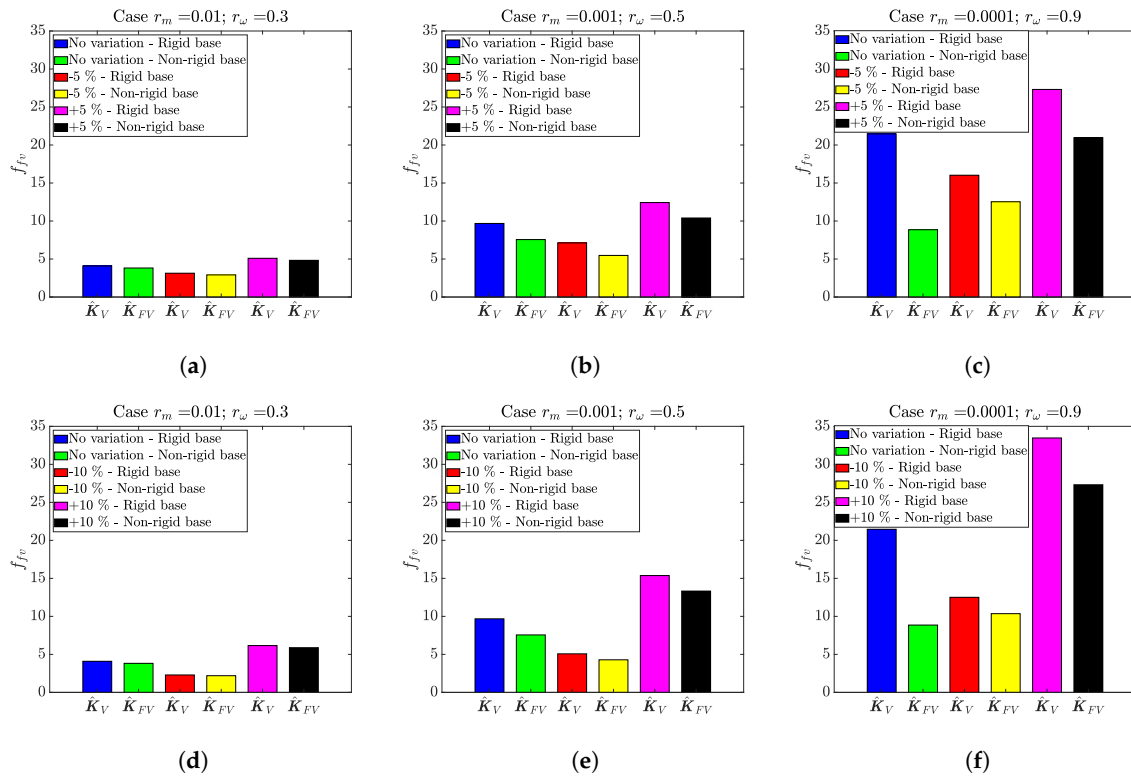


Figure 12. Effect on the VI and alignment performance of 5% variation (a–c) and 10% variation (d–f) in the dynamic parameters $\zeta_{p_2}, \omega_{p_2}$ of the mid-span isolator—non-symmetrical case.

5. Conclusions

This work describes the theoretical development of a new control scheme for multi-isolator scenarios aimed at delivering excellent vibration isolation as well as alignment of multiple devices supported by a single flexible structure. The efficacy of the proposed AVI scheme is demonstrated via extensive simulations on a three-isolator systems supported by a pinned-pinned beam. Both symmetrical and non-symmetrical configurations of the isolators are analyzed. The analysis highlights the importance of considering the dynamics of the supporting structure during the control design. key conclusions of this analyses are: (i) the best isolator in terms of transmissibility is not the optimum when component alignment is considered; (ii) the influence of supporting structure dynamics on control design and resulting performance is more pronounced for low mass ratios; (iii) there is a trade-off between the transmissibility and vibration cancellation of the supporting structure; (iv) this trade-off also depends on how the vibration modes are excited (by the disturbance forces) and are cancelled (by the isolators); and (v) the contribution of the vibration modes may produce large differences between the rigid and non-rigid hypotheses, as illustrated in the three disturbance force cases. The proposed scheme possesses adequate robustness for practical implementation, as shown by the parametric analysis results presented for parameter uncertainty in the mid-span isolator. Future work will focus on experimental validation and optimization based on actuators with complimentary bandwidths.

Author Contributions: Conceptualization, J.P.-A. and E.P.; methodology, J.P.-A. and E.P.; software, J.P.-A.; validation: J.P.-A., E.P., S.S.A. and P.R.; formal analysis, E.P. and P.R.; investigation, J.P.-A., E.P., S.S.A. and P.R.; resources, J.P.-A.; data curation, J.P.-A.; writing—original draft, J.P.-A.; preparation, J.P.-A.; writing—review and editing, E.P., S.S.A. and P.R.; visualization, J.P.-A.; supervision, E.P., S.S.A. and P.R.; project administration, E.P. and P.R.; and funding acquisition, P.R. All authors have read and agreed to the published version of the manuscript.

Funding: This work was funded by the University of Exeter (UoE), and the College of Engineering, Mathematics, and Physical Sciences (CEMPS).

Acknowledgments: The authors would like to thank the editors and anonymous reviewers for their useful comments.

Conflicts of Interest: The authors declare no conflict of interest.

Abbreviations

The following abbreviations are used in this manuscript:

VI	Vibration Isolation
PVI	Passive Vibration Isolation
SAVI	Semi-Active Vibration Isolation
AVI	Active Vibration Isolation
SISO	Single-Input-Single-Output
MIMO	Multiple-Input-Multiple-Output

References

1. Preumont, A. *Vibration Control of Active Structures*; Springer: Berlin/Heidelberg, Germany; New York, NY, USA, 2018.
2. Rivin, E.I. *Passive Vibration Isolation*; ASME Press: New York, NY, USA, 2003.
3. Liu, Y.; Waters, T.; Brennan, M. A Comparison of Semi-Active Damping Control Strategies for Vibration Isolation of Harmonic Disturbances. *J. Sound Vib.* **2005**, *280*, 21–39. [[CrossRef](#)]
4. Jansen, L.M.; Dyke, S.J. Semiactive Control Strategies for MR Dampers: Comparative Study. *J. Eng. Mech.* **2000**, *126*, 795–803. [[CrossRef](#)]
5. Gavin, H.P.; Alhan, C. Guidelines for Low-Transmissibility Semi-Active Vibration Isolation. *Smart Mater. Struct.* **2005**, *14*, 297–306. [[CrossRef](#)]
6. Rossi, A.; Orsini, F.; Scorza, A.; Botta, F.; Belfiore, N.; Sciuto, S. A Review on Parametric Dynamic Models of Magnetorheological Dampers and Their Characterization Methods. *Actuators* **2018**, *7*, 16. [[CrossRef](#)]
7. Ibrahim, R. Recent Advances in Nonlinear Passive Vibration Isolators. *J. Sound Vib.* **2008**, *314*, 371–452. [[CrossRef](#)]
8. Ho, C.; Lang, Z.Q.; Sapiński, B.; Billings, S.A. Vibration Isolation Using Nonlinear Damping Implemented by a Feedback-Controlled MR Damper. *Smart Mater. Struct.* **2013**, *22*, 105010. [[CrossRef](#)]
9. Lu, Z.; Brennan, M.J.; Chen, L.Q. On the Transmissibilities of Nonlinear Vibration Isolation System. *J. Sound Vib.* **2016**, *375*, 28–37. [[CrossRef](#)]
10. Wang, S.; Gao, P.; Hu, Y.; Li, B. A Novel Dual-Parallelogram Passive Rocking Vibration Isolator: A Theoretical Investigation and Experiment. *Appl. Sci.* **2017**, *7*, 367. [[CrossRef](#)]
11. Song, Y.; Sun, X. Modeling and Dynamics of a MDOF Isolation System. *Appl. Sci.* **2017**, *7*, 393. [[CrossRef](#)]
12. Dong, Y.Y.; Han, Y.W.; Zhang, Z.J. On the Analysis of Nonlinear Dynamic Behavior of an Isolation System with Irrational Restoring Force and Fractional Damping. *Acta Mech.* **2019**, *230*, 2563–2579. [[CrossRef](#)]
13. Lu, Z.Q.; Gu, D.H.; Ding, H.; Lacarbonara, W.; Chen, L.Q. Nonlinear Vibration Isolation via a Circular Ring. *Mech. Syst. Signal Process.* **2020**, *136*, 106490. [[CrossRef](#)]
14. Bouna, H.S.; Nbandjo, B.R.N.; Wofo, P. Isolation Performance of a Quasi-Zero Stiffness Isolator in Vibration Isolation of a Multi-Span Continuous Beam Bridge under Pier Base Vibrating Excitation. *Nonlinear Dyn.* **2020**, *100*, 1125–1141. [[CrossRef](#)]
15. Marneffe, B.D.; Avraam, M.; Deraemaeker, A.; Horodincu, M.; Preumont, A. Vibration Isolation of Precision Payloads: A Six-Axis Electromagnetic Relaxation Isolator. *J. Guid. Control. Dyn.* **2009**, *32*, 395–401. [[CrossRef](#)]
16. Ruzicka, J.E. Active Vibration and Shock Isolation. In Proceedings of the National Aeronautic and Space Engineering and Manufacturing Meeting, Los Angeles, CA, USA, 7–11 October 1968. [[CrossRef](#)]
17. Preumont, A.; Horodincu, M.; Romanescu, I.; de Marneffe, B.; Avraam, M.; Deraemaeker, A.; Bossens, F.; Abu Hanieh, A. A Six-Axis Single-Stage Active Vibration Isolator Based on Stewart Platform. *J. Sound Vib.* **2007**, *300*, 644–661. [[CrossRef](#)]
18. Bastaits, R.; Rodrigues, G.; Mokrani, B.; Preumont, A. Active Optics of Large Segmented Mirrors: Dynamics and Control. *J. Guid. Control. Dyn.* **2009**, *32*, 1795–1803. [[CrossRef](#)]

19. Kong, Y.; Huang, H. Vibration Isolation and Dual-Stage Actuation Pointing System for Space Precision Payloads. *Acta Astronaut.* **2018**, *143*, 183–192. [[CrossRef](#)]
20. Chen, S.; Xuan, M.; Xin, J.; Liu, Y.; Gu, S.; Li, J.; Zhang, L. Design and Experiment of Dual Micro-Vibration Isolation System for Optical Satellite Flywheel. *Int. J. Mech. Sci.* **2020**, *2020*, 105592. [[CrossRef](#)]
21. Beard, A.M.; Schubert, D.W.; von Flotow, A.H. Practical Product Implementation of an Active/Passive Vibration Isolation System. In *Vibration Monitoring and Control*; International Society for Optics and Photonics: Bellingham, WA, USA, 1994; Volume 2264. [[CrossRef](#)]
22. Nakano, K.; Suda, Y.; Nakadai, S. Self-Powered Active Vibration Control Using a Single Electric Actuator. *J. Sound Vib.* **2003**, *260*, 213–235. [[CrossRef](#)]
23. Liu, C.; Jing, X.; Daley, S.; Li, F. Recent Advances in Micro-Vibration Isolation. *Mech. Syst. Signal Process.* **2015**, *56–57*, 55–80. [[CrossRef](#)]
24. Preumont, A.; FrançOis, A.; Bossens, F.; Abu-Hanieh, A. Force Feedback versus Acceleration Feedback in Active Vibration Isolation. *J. Sound Vib.* **2002**, *257*, 605–613. [[CrossRef](#)]
25. Beijen, M.; Heertjes, M.; Butler, H.; Steinbuch, M. H_∞ Feedback and Feedforward Controller Design for Active Vibration Isolators. *IFAC-PapersOnLine* **2017**, *50*, 13384–13389. [[CrossRef](#)]
26. Beijen, M. Disturbance Feedforward Control for Vibration Isolation Systems: Analysis, Design, and Implementation. Ph.D. Thesis, Technische Universiteit Eindhoven, Eindhoven, The Netherlands, 2018.
27. Kaplow, C.; Velman, J. Active Local Vibration Isolation Applied to a Flexible Space Telescope. *J. Guid. Control. Dyn.* **1980**, *3*, 227–233. [[CrossRef](#)]
28. Wang, C.; Xie, X.; Chen, Y.; Zhang, Z. Active Vibration Isolation through a Stewart Platform with Piezoelectric Actuators. *J. Phys. Conf. Ser.* **2016**, *744*, 012006. [[CrossRef](#)]
29. Mikhailov, V.P.; Bazinenkov, A.M. Active Vibration Isolation Platform on Base of Magnetorheological Elastomers. *J. Magn. Magn. Mater.* **2017**, *431*, 266–268. [[CrossRef](#)]
30. Inman, D. Control/Structure Interaction—Effects of Actuator Dynamics. In *Dynamics Specialists Conference*; American Institute of Aeronautics and Astronautics: Long Beach, CA, USA, 1990. [[CrossRef](#)]
31. Huang, X.; Elliott, S.; Brennan, M. Active Isolation of a Flexible Structure from Base Vibration. *J. Sound Vib.* **2003**, *263*, 357–376. [[CrossRef](#)]
32. Liu, J.; Liu, H.J.; Dyke, S.J. Control–Structure Interaction for Micro-Vibration Structural Control. *Smart Mater. Struct.* **2012**, *21*, 105021. [[CrossRef](#)]
33. Farshidianfar, A.; Saghafi, A.; Kalami, S.M.; Saghafi, I. Active Vibration Isolation of Machinery and Sensitive Equipment Using H_∞ Control Criterion and Particle Swarm Optimization Method. *Meccanica* **2012**, *47*, 437–453. [[CrossRef](#)]
34. Venanzi, I.; Ierimonti, L.; Ubertaini, F. Effects of Control-Structure Interaction in Active Mass Driver Systems with Electric Torsional Servomotor for Seismic Applications. *Bull. Earthq. Eng.* **2017**, *15*, 1543–1557. [[CrossRef](#)]
35. Jiang, J.; Gao, W.; Wang, L.; Teng, Z.; Liu, Y. Active Vibration Control Based on Modal Controller Considering Structure-Actuator Interaction. *J. Mech. Sci. Technol.* **2018**, *32*, 3515–3521. [[CrossRef](#)]
36. Alujević, N.; Senjanović, I.; Čatipović, I.; Vladimir, N. The Absence of Reciprocity in Active Structures Using Direct Velocity Feedback. *J. Sound Vib.* **2019**, *438*, 251–256. [[CrossRef](#)]
37. Allaoua, S.; Guenfaf, L. LQG Vibration Control Effectiveness of an Electric Active Mass Damper Considering Soil–Structure Interaction. *Int. J. Dyn. Control* **2019**, *7*, 185–200. [[CrossRef](#)]
38. Li, M.; Zhang, Y.; Wang, Y.; Hu, Q.; Qi, R. The Pointing and Vibration Isolation Integrated Control Method for Optical Payload. *J. Sound Vib.* **2018**, *438*, 441–456. [[CrossRef](#)]
39. Elliott, S.; Benassi, L.; Brennan, M.; Gardonio, P.; Huang, X. Mobility Analysis of Active Isolation Systems. *J. Sound Vib.* **2004**, *271*, 297–321. [[CrossRef](#)]
40. Sciulli, D.; Inman, D.J. Isolation Design for a Flexible System. *J. Sound Vib.* **1998**, *216*, 251–267. [[CrossRef](#)]
41. Chopra, K.A. *Dynamic of Structures*, 4th ed.; Pearson: London, UK, 2011.

42. Lagarias, J.C.; Reeds, J.A.; Wright, M.H.; Wright, P.E. Convergence Properties of the Nelder–Mead Simplex Method in Low Dimensions. *SIAM J. Optim.* **1998**, *9*, 112–147. [[CrossRef](#)]
43. D’Errico, J. *Fminsearchbnd*, *Fminsearchcon*; MathWorks: Natick, MA, USA, 2020.

Publisher’s Note: MDPI stays neutral with regard to jurisdictional claims in published maps and institutional affiliations.



© 2020 by the authors. Licensee MDPI, Basel, Switzerland. This article is an open access article distributed under the terms and conditions of the Creative Commons Attribution (CC BY) license (<http://creativecommons.org/licenses/by/4.0/>).